J. Non-Newtonian Fluid Mech. 166 (2011) 32–41

Contents lists available at ScienceDirect

Journal of Non-Newtonian Fluid Mechanics

journal homepage: www.elsevier.com/locate/jnnfm

Bubble cluster formation in shear-thinning inelastic bubbly columns

J. Rodrigo Vélez-Cordero, Roberto Zenit*

Instituto de Investigaciones en Materiales, Universidad Nacional Autónoma de México, Circuito Exterior s/n, Apdo. Postal 70-360 México D.F. 04510, Mexico

ARTICLE INFO

Article history:
Received 13 July 2010
Received in revised form
27 September 2010
Accepted 8 October 2010

Keywords:
Bubbly flows
Non-Newtonian
Shear-thinning
Clusters

ABSTRACT

The mean rise velocity of bubble swarms ascending in shear-thinning fluids was experimentally measured in a rectangular bubble column. Great care was taken to produce nearly mono-dispersed bubble swarms and to use shear-thinning fluids with negligible elastic effects. In this manner, it was possible to isolate the effect of the hydrodynamic interaction between bubbles in the column caused by the thinning behavior of the liquid. It was found that the mean rise velocity of the bubbles was larger than that of an individual bubble, in accordance with previous studies. The magnitude of the swarm velocity was found to be greatly influenced by the appearance of bubble clusters. The bubble clusters, which appeared for certain values of the flow index and bubble diameter, were found to have a very different structure from those observed in Newtonian liquids. Furthermore, it was found that the appearance of clusters produced a dramatic increase of the agitation within the column. A set of conditions was identified for the appearance of bubble clusters in shear-thinning inelastic bubbly columns.

1. Introduction

One of the greatest challenges in fluid dynamics is to understand and predict the behavior of multiphase flow systems. This is a task that is widely justified due to the occurrence of gas–liquid/gas–liquid–solid contactors in almost every branch of the chemical and metallurgical industries. In particular, bubble columns are used in many chemical processes which involve oxidation, chlorination, polymerization and hydrogenation [1–3], to name a few. Bubble columns are also used as a central unit operation for primary and secondary metabolites production and for several downstream processes for product recovery such as the separation by adsorption in bubble flows [1,4,5]. In spite of the mechanical simplicity that characterizes bubble columns, which grant them with operative and cost benefits [6], their basic engineering design is not a simple task. Given a certain chemical process and liquid phase properties, an engineer has to implement the optimum column geometry, sparger configuration and power input (superficial gas velocity U_g) to satisfy the uptake rate of the ongoing chemical reaction, in addition to achieving the optimum mixing and heat transfer properties between phases. Such estimations require the knowledge of functional relations among the central operational variables such as the mean bubble diameter $\bar{d}_b$, mean bubble velocity $\bar{U}_{SW}$ and gas fraction Φ_g. Some authors have also studied the development of the liquid velocity and its variance as a measure of the amount of agitation or *pseudo-turbulence* conferred by the dispersed phase [7,8]. Deeper understanding of bubble–bubble and bubble–liquid interactions require the use of computational fluid dynamics in which one can easily choose and manipulate the field variables [9–11].

Although many industrial liquids which comprise solutions of low molecular weight can be considered Newtonian-like fluids, an increasing number of solutions with high molecular weights and internal structure are being used that have non-Newtonian behavior such as variable viscosity and memory effects. Polymer solutions and melts, liquid crystals, gels, suspensions, emulsions, micellar solutions, slurries and foams enter into this non-Newtonian category [10,12]. The study of non-Newtonian effects in the behavior of bubble flows is, therefore, of fundamental importance.

Experimental and numerical studies in two phase flows (including sedimentation and bubble flows) have shown that a group of bodies moving through a non-Newtonian fluid tend to form aggregates or clusters [11,13–15]. Such aggregates are more dense in terms of the number of bubbles embedded in the bubble cloud than the clusters that have been described in Newtonian flows at high Reynolds numbers [16,17]; actually, we will show in this study that bubbles rising in shear-thinning fluids group with each other forming aggregates of a certain size. Bubble clustering cause bubble coalescence and a premature transition to the heterogeneous or churn-turbulent flow in non-Newtonian fluids [18,19]. Although there has been a number of studies of particle clustering and orientation of lengthened bodies in sedimentation [15,14,22], little has been reported for the case of bubbly flows. The aim of the present work is to study the formation of clusters of mono-disperse bubbles in power-law shear-thinning fluids, leaving aside, as much as possible, the elastic effects. We support the discussion of our

* Corresponding author. Tel.: +52 55 5622 4593; fax: +52 55 5622 4602.
E-mail address: zenit@servidor.unam.mx (R. Zenit).

0377-0257/$ – see front matter © 2010 Elsevier B.V. All rights reserved.
doi:10.1016/j.jnnfm.2010.10.003

experimental observations with the results of a companion paper [23] which analyzes the hydrodynamic interaction between bubble pairs ascending in shear-thinning fluids, both experimentally and numerically.

2. Background

Most of the published papers on non-Newtonian bubble columns have focused their attention on the development of the gas fraction, Φ_g, in terms of the superficial gas velocity, U_g. Many authors have used CMC (carboxymethylcellulose) solutions (flow index $n > 0.5$) [18,19,24–27] in coalescence conditions and worked with relatively large values of the superficial gas velocity ($U_g > 2$ cm/s) [25–27] such that the churn-turbulent flow was generally achieved.

Buchholz et al. [18] reported that the mean bubble rise velocity $\bar{U}_{SW}$ measured in a single stage column was higher than the single bubble velocity U_{SI}. Additionally, this difference increased with the thinning behavior of the fluid. However, the changes of the $\bar{U}_{SW}/U_{SI}$ ratio with the gas fraction were not reported explicitly. Schumpe and Deckwer [19] found that the homogeneous bubble regime in CMC solutions could only be achieved having U_g values below a critical one (~0.5 cm/s), this value being a function of the effective viscosity. Haque et al. [26,27] reported an estimation of the mean bubble diameter and velocity of bubble swarms rising in viscoelastic fluids. One of the key assumptions in this estimation is that the mean bubble velocity values are equal to the single bubble velocity, which is not always true. As far as we know, there are no previous studies of mono-dispersed bubble swarms in shear-thinning fluids at low superficial gas velocities ($U_g < 1$ cm/s) where the bubbly flow regime can be observed. Having a monodispersed bubble distribution allows us to isolate the effects caused solely by the hydrodynamic interaction among bubbles.

Many relevant contributions to the subject have arisen from numerical and analytical studies. Several methods such as variational principles [28], perturbation methods [29] and approximations to the Newtonian behavior [30] have been used to solve numerically the rising of a bubble or bubble swarms through shear-thinning fluids. Bubble interactions were simplified using the Happel cell model [31], hence no direct bubble interactions have been studied previously. Only Radl et al. [11] have fully resolved the flow field around a group of bubbles. Bhavaraju et al. [29] reported that for creeping flow conditions the drag coefficient C_d decreased with the increase of the thinning behavior for bubble swarms, which is the opposite of what happens for single bubbles. Ascending isolated bubbles have a larger C_d as the thinning condition increases [27,30,32,33]. In more recent studies, which took into account the inertial forces in the momentum equation [10,34], this increase in the drag force for the single bubble cases occurred only below a critical Reynolds number (approximately from 3 to 10). Gummalam and Chhabra [28,35] reported that for the creeping and high Re numbers ($100 < Re < 300$) flows, the $\bar{U}_{SW}/U_{SI}$ ratio increases for gas fractions below 0.3 and flow index values below 0.5. Above this gas fraction value the velocity ratio decreases. Therefore, a maximum in the velocity ratio was observed for $\Phi_g \approx 0.3$. These authors explained that such behavior is due to the constrain of the flow lines (as the effective volume for each bubble is decreased as the gas fraction increases) resulting in an increase of the shear rate which in turn results in lower apparent viscosities. A positive slope of the velocities ratio curve means that the viscosity gradients effects surpass the hydrodynamic hindrance effects. The slope of the $\bar{U}_{SW}/U_{SI}$ curve is commonly negative in Newtonian bubbly liquids with large Reynolds and small Weber numbers [17,36]. It is important to point out that the theoretical results of Refs. [28,29,35] have not been compared with experiments yet.

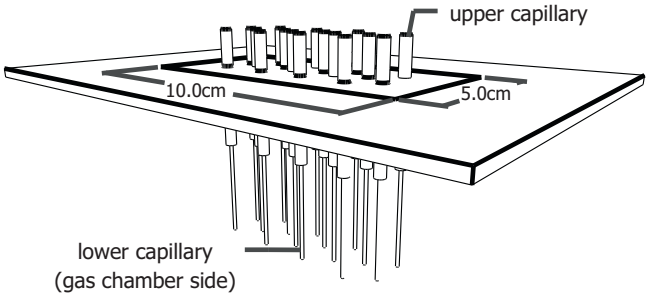

Fig. 1. Scheme of a capillary bank.

Radl et al. [11] directly simulated the interactions of bubbles (up to 9) rising in shear-thinning conditions. They showed that the bubble interactions are significantly enhanced when viscosity gradients are present. They also identified *"mini-bubble"* clusters that travel faster than the single bubble cases. This feature will be discussed in depth in the present investigation.

In this work, we compared the $\bar{U}_{SW}/U_{SI}$ values obtained in the bubble column at different gas fractions and thinning conditions with the theoretical ones [28,35]. We also conducted an analysis of the size of bubble clusters and of the bubble velocity variance. Finally, we identified the hydrodynamic conditions for which bubble clusters are formed.

3. Experimental setup

3.1. Bubble column and capillary banks

A rectangular channel with $5 \times 10 \times 160\,\text{cm}^3$ equipped with a gas chamber (7.5% of the channel height) was used, similar to that used by Martínez-Mercado et al. [8]. Pure nitrogen was introduced to the bubble column using a needle valve (*Cole-Palmer 1682 ml/min MAX, stainless steel ball*). The superficial gas velocity U_g range was between 0.09 and 0.6 cm/s. The gas volume fraction, Φ_g, was obtained using the relation $\Phi_g = \Delta H/H$, where H is the liquid height without gas (140 cm) and ΔH the height difference produced by the introduction of the gas in the column.

Three capillary banks were constructed in order to produce different bubble sizes (d_b). The internal diameter of the capillaries (D_{cap}) was selected considering the equilibrium condition between buoyancy and surface tension forces:

$$D_{\text{cap}} = \frac{{d_b}^3 \rho g}{6\sigma} \tag{1}$$

where ρ is the liquid density, g the gravity and σ the surface tension.

In order to avoid the generation of gas jets with variable volume, the hydraulic resistance through the capillaries should be large such that the bubble volume depends mainly on the buoyancy and surface forces and lesser in the gas flow rate [37]. The equivalent capillary lengths necessary to achieve such hydraulic resistance are sometimes of the order of meters; instead of installing long capillaries, a second capillary with a smaller inner diameter was inserted to the main capillary but the bubble formed on the larger diameter end. This arrangement provides the sufficient pressure drop to produce individual bubbles. As we can see in Fig. 1, identical capillaries were placed in an acrylic perforated plate ordered in an hexagonal arrange. The design parameters of the three capillary banks are summarized in Table 1.

3.2. Fluids

The fluids used in this study fulfilled two conditions: (1) show a shear-thinning power-law behavior with negligible elastic proper-

Table 1
Design parameters of the capillary banks. D_{cap}, internal diameter of the capillaries; N, number of capillaries; $\bar{d}_b$, experimental mean bubble diameter; λ, spacing between capillaries; λ_{wall}, spacing between capillaries and the wall; L, capillary length.

	D_{cap} (mm)	N	$\bar{d}_b$ (mm)	$\lambda/\bar{d}_b$	$\lambda_{wall}/\bar{d}_b$	L (cm)
1	0.2	63	2.15	2.8	6.7	4.3
2	0.6	27	3.15	2.7	4.9	8.0
3	1.6	16	4.20	2.7	3.7	8.0

ties and (2) allow the formation of mono-dispersed bubbly flows, that is, with a narrow dispersion of $\bar{d}_b$.

It was found that xanthan gum solutions in a water/glycerin mixture fulfilled the above conditions. These solutions are more stable in the presence of $MgSO_4$ (which was added to delay coalescence [38]) than carbopol, CMC or guar gum solutions. The preparation of the solutions was as follows: first the xanthan gum (*Keltrol E 415, KELCO, USA*) was dissolved in water (at 55 °C), then the salt (0.04 M of $MgSO_4$, *2500-01 J.T. Baker*) was added and finally the glycerin. The solutions were left in repose for 24 h before experiments. The rheological measurements were done in a rheometer (*TA Instruments AR1000N*) with a cone-plate geometry (60 mm, 2 °, a gap of 65 μm). The surface tension measurements were performed with a DuNouy ring (diameter of 19.4 mm, *KSV Sigma 70*). All the solutions were stirred before the surface tension measurement. The temperature of the room was 23 °C. The physical properties of the solutions are summarized in Table 2; the flow curves are shown in Fig. 2. The data contained in this figure includes measurements performed one and two weeks after the preparation of the fluids.

At a shear rate of 10 s^{-1} all the fluids have a viscosity of around one hundred times that of water. The shear-thinning fluids have a power-law behavior in almost all the shear rate interval; a mild plateau can be observed for shear rates below 0.1 s^{-1}. This indicates that the polymer chains are gently stretched by a flow field, having a short range of linear viscoelasticity. Within this short linear range, the elastic modulus G' becomes bigger than the loss modulus G'' only at high frequencies (>100 s^{-1}) as can be seen in Fig. 3. Both G' and G'' were obtained by a Fourier Transform (FT) of the stress relaxation curves measured with an *ARG2* rheometer of controlled stress [39]. The normal forces (first normal stress difference) of the thinning fluids, measured with the cone-plate geometry, reach a maximum value of 7 Pa at 100 s^{-1} but decreased as the shear rate increased (data not shown). This behavior contrasts with the one shown by a viscoelastic fluid (a 0.2% polyacrylamide solution can reach a normal stress value of 100 Pa for the same range of shear rates) or an upper-convected Maxwell fluid where the normal stress grows as a function of $\dot{\gamma}^2$; clearly the behavior of our fluids is very different. With these fluids (and with their rheological characterization) we were able to isolate, as much as possible, the thinning effects from the elastic ones over a wide range of characteristic flow times. We can expect then that the hydrodynamic behavior of bubble–bubble interactions is mainly attributed to the shear-thinning behavior.

3.3. Bubble diameters and velocities measurements

For the measurements of the mean bubble diameters, $\bar{d}_b$, and the mean bubble velocities, $\bar{U}_{SW}$, a high speed camera (*MotionScope PCI 8000s*) was used. A recording rate of 500 frames/s and a shutter speed of 1/1000 was used. The camera was positioned 20 cm below the liquid surface facing the larger side of the bubble column. Two different videos were obtained per experiment: one for the $\bar{d}_b$ measurements, where the camera was placed 120 cm from the bubble column (using a 105 mm objective lens) and another for the bubble velocity measurements, where the camera was placed a little bit farther, 180 cm from the bubble column (using a 60 mm objective lens). Diffuse back light was used, with a light source placed at 90 ° from the camera direction and reflected by a panel. The video frames were converted to binary format and analyzed using a conventional image processor software (Matlab©). The equivalent mean bubble diameter $\bar{d}_b$ was calculated using the measurement of the short and long diameters of the elliptic bubble projections:

$$\bar{d}_b = (\bar{d}^2_{MAX}\bar{d}_{MIN})^{1/3} \quad (2)$$

where $\bar{d}_{MAX}$ is the larger bubble diameter and $\bar{d}_{MIN}$ the shorter bubble diameter. In some bubbly flows an equivalent mean cluster diameter was also measured. Although clusters shapes are highly irregular, an estimation of its size was made using Eq. (2), now tak-

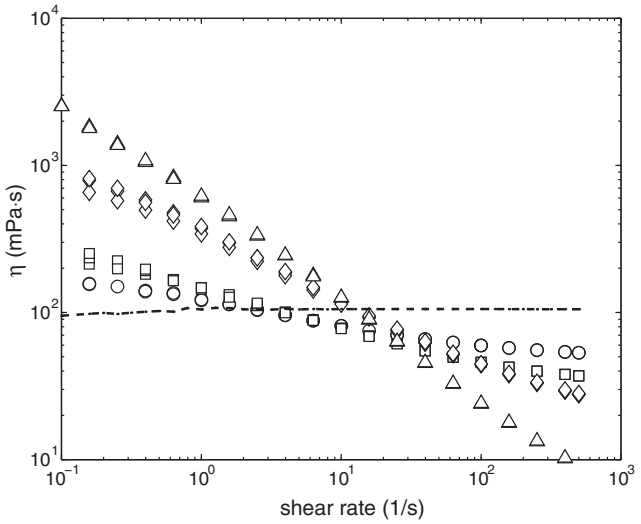

Fig. 2. Flow curves of the test fluids. η: apparent viscosity, (– –) Newtonian fluid, (○) $n = 0.85$, (□) $n = 0.76$, (◊) $n = 0.55$, (△) $n = 0.32$.

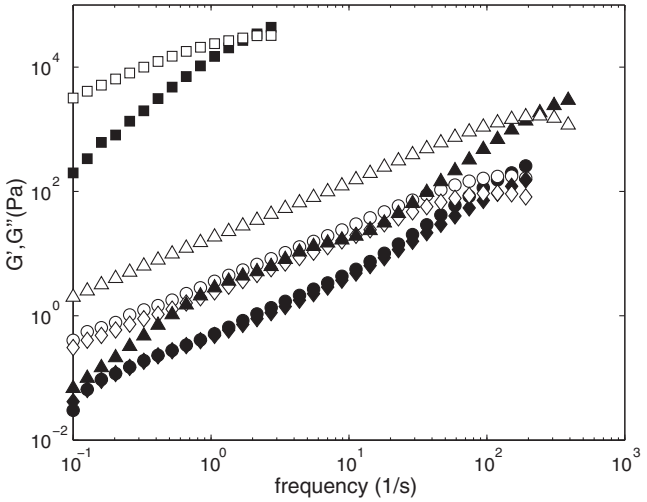

Fig. 3. Dynamic moduli of three shear thinning solutions. Filled symbols: elastic modulus G'; empty symbols: loss modulus G''; (○) $n = 0.85$, (◊) $n = 0.55$, (△) $n = 0.32$, (□) a polyacrylamide reference solution (0.04% in 80% glycerin/water with 0.04 M $MgSO_4$). For the estimation of G' and G'' the procedure followed by Calderas et al. [39] was used.

Table 2
Physical properties of the fluids: ρ, density; σ, surface tension; η, viscosity; k, consistency index; n, flow index. The percentages of liquid mixtures are given in volume terms, the percentages of the xanthan gum solutions in weight terms. In all the fluids 0.04 M of $MgSO_4$ was added to delay bubble coalescence.

Fluids	ρ (kg/m^3)	σ (mN/m)	η or k (mPa s^n)	n
Newtonian: 83% glycerin/water	1214.6	61.9	104.2	1.0
0.02% Xanthan gum in 75% glycerin/water	1193.1	63.0	118.7	0.85
0.035% Xanthan gum in 70% glycerin/water	1179.5	62.0	143.4	0.76
0.1% Xanthan gum in 60% glycerin/water	1152.1	65.0	360.0	0.55
0.23% Xanthan gum in water	997.5	66.5	574.9	0.32

ing the longer and shorter diameters of the cluster. The reported $\bar{U}_{SW}$ values were the average of the vertical component of the velocity vector. At least 100 measurements were done for each experimental condition. When bubble aggregates appeared, we measured the velocity of individual bubbles located at the periphery of the clusters; these were more easy to recognize than the bubbles located in the interior of the cluster. The fluids were discarded after one week of experimental work. The whole column was disassembled and cleaned at the end of the day.

The velocity and size of isolated bubbles were also measured covering a bubble volume range from 0.1 to 100 mm^3. Such measurements were done in a cylindrical column with an inner diameter of 9 cm equipped with a bubble dispenser similar to the one used by Soto et al. [40].

4. Experimental results

4.1. Single bubbles

The values of the drag coefficient, C_d, of the individual bubbles as a function of the Reynolds number, Re, are shown in Fig. 4. The Reynolds number and drag coefficient were defined as:

$$Re = \frac{\rho U_{SI} d_b}{\eta} \tag{3}$$

where

$$\eta = k\left(\frac{2U_{SI}}{d_b}\right)^{n-1} \tag{4}$$

and

$$C_d = \frac{4}{3}\frac{d_b g}{U_{SI}^2} \tag{5}$$

In addition to the common functional dependence of the drag coefficient on the Reynolds number in the laminar flow regime, we can also observe that the C_d values found for the thinning fluids are higher than those found for the Newtonian fluid. This increase of the drag coefficient with the thinning behavior has been already reported by theoretical [30,29], experimental [29,27] and numerical [23] studies for the creeping and small but finite Reynolds regimes. Note that for the Newtonian fluid the Oseen wake is already seen at $Re \sim 7$. With these measurements, the accuracy of our experimental results was verified. Although we cannot state that our fluids are totally free from elastic effects, i.e. the flow around a bubble is complex so memory effects can rise from extensional flow; the fact that we did not observe any signal of a velocity jump discontinuity supports the statement that the elastic effects were very small indeed.

4.2. Bubbly flow regime and cluster formation

As pointed out by other authors [18,19] the transition from bubbly to the heterogeneous regime, which is characterized by the presence of multi-dispersed bubble swarms, can be identified by a change in the slope of the gas volume fraction as a function of the superficial gas velocity. The slope of the curve changes (decreases) as a consequence of the change of the bubble volume. In Fig. 5 the gas fraction value is shown as a function of the superficial gas velocity for the Newtonian and a thinning fluid ($n = 0.85$) for several bubble diameters. For both cases the mean bubble size produced by each capillary bank was practically the same.

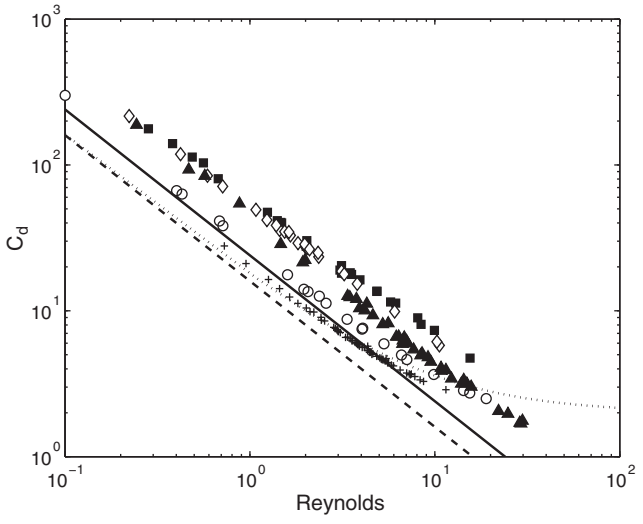

Fig. 4. Drag coefficient as a function of the Reynolds number for the single bubbles. (+) Newtonian fluid, (○) $n = 0.85$, (■) $n = 0.76$, (◊) $n = 0.55$, (▲) $n = 0.32$, (−) Stokes prediction, (− −) Hadamard prediction, (. . .) Oseen correction for a fluid sphere $C_d = 16/Re + 2$.

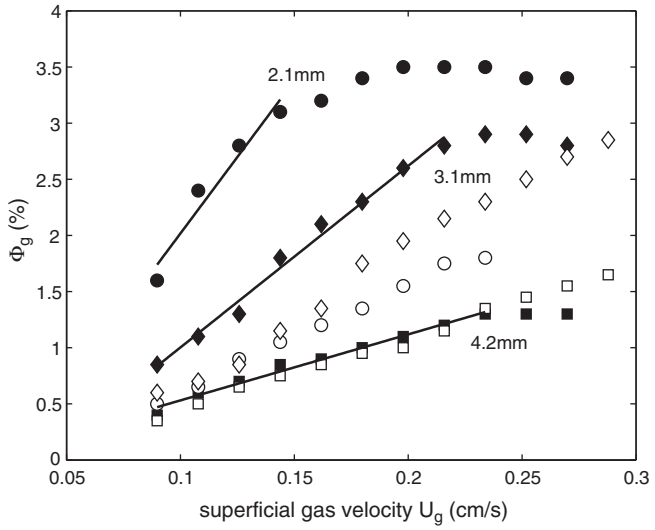

Fig. 5. Gas fraction values as a function of the superficial gas velocity. Filled symbols: Newtonian fluid, empty symbols: $n = 0.85$ fluid, (○) $\bar{d}_b = 2.1$ mm, (◊) $\bar{d}_b = 3.1$ mm, (□) $\bar{d}_b = 4.2$ mm.

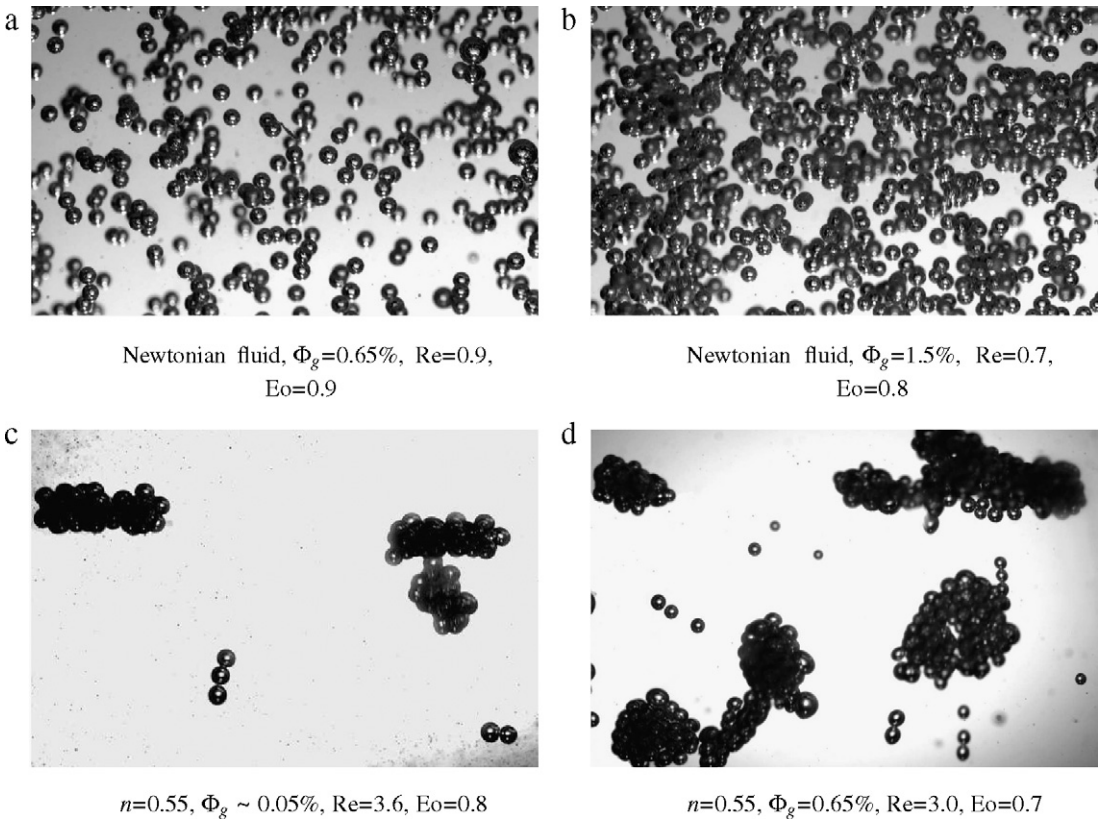

Fig. 6. Bubbly flow pictures taken at different gas fraction values for the Newtonian fluid and the $n = 0.55$ thinning fluid. The magnification of the images is approximately the same. The image size is about $5 \times 3\ cm^2$. The bubble size (2.1 mm) correspond to the one produced by the smallest capillary diameter. The Reynolds number was computed using the mean bubble diameter and velocity of the bubbly flow. The Eötvös (Eo) number is defined below.

For the Newtonian case (filled symbols) the bubbles with the smaller $\bar{d}_b$ produce higher gas fraction values, as expected. The transition to the heterogeneous flow can be seen by the change of the linear slope of the curves for the three different bubble diameters. The Φ_g values obtained for the thinning fluid are similar to the Newtonian case for 3.1 and 4.2 mm bubble diameters; for the smaller bubbles (2.1 mm) the gas fraction values are clearly below the Newtonian ones; this is due to the presence of bubble clusters, as we will show below. Note that with the other bubble diameters, where no bubble cluster were found, the transition to the heterogeneous regime was observed at higher values of U_g with respect to the Newtonian fluid. All the measurements reported hereafter in this paper were taken before the transition to the heterogeneous regime.

Fig. 6 shows images of the bubbly flows produced with the present setup. The images correspond to the Newtonian fluid and to the shear-thinning fluid with $n = 0.55$ for the smallest bubble size. The formation of large bubble aggregates in the thinning fluid is largely evident (Fig. 6c and d). The difference with the Newtonian case (Fig. 6a and b) is striking.

While the orientation of such clusters is mainly horizontal, spheroidal clusters and small bubble chaining can also be seen. It is worthwhile to mention that the clusters are not static while rising through the fluid; on the contrary, they have a dynamic structure. A careful observation reveals that the bubbles move in toroidal trajectories, rising in the center and descending on the exterior part of the cluster. As the gas fraction increases, just before the regime transition, the bubbles embedded in such clusters inevitably coalesce and form large cap bubbles.

A similar toroidal or periodic movement has also been observed in the case of settling particles forming clusters at low Re [20,21]. Nevertheless, besides the difference between the degree of deformation, such periodic movement seen in Newtonian fluids disappear as soon as inertia ($Re > 0.2$) or the number of particles (around 7) are increased. Fig. 6 clearly shows that clustering in thinning fluids appears above these limiting factors.

4.3. Bubble size distribution

Fig. 7 shows the histogram of the bubble diameter for the Newtonian fluid and the $n = 0.76$ fluid; the plot shows data taken for each

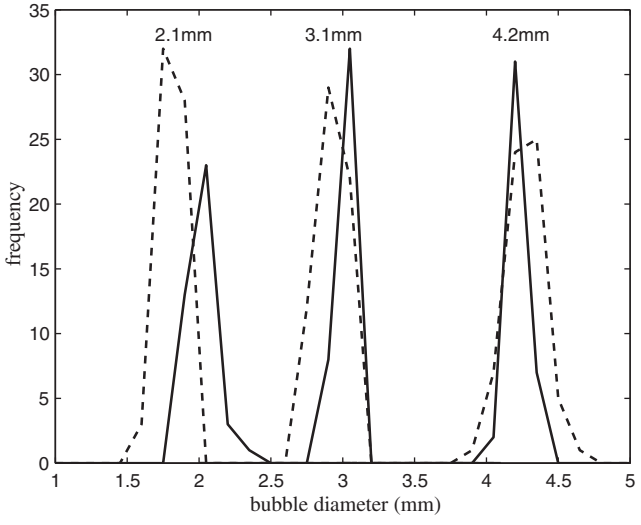

Fig. 7. Histograms of the equivalent mean bubble diameters $\bar{d}_b$ for the Newtonian (–) and $n = 0.76$ (– –) fluids produced by the three capillary banks; 15 classes were used to sort the bubble diameters. The frequency refers to the number of values found in each class.

capillary bank. In both cases the curves show a narrow distribution of the bubbles diameters produced by the capillary banks indicating that the formation of nearly mono-dispersed bubbly flows was accomplished. In addition, it can be seen that the bubble diameter distributions are similar for both cases, indicating that the different fluids used in this work allowed the formation of bubbles with similar mean bubble diameters. The same behavior was observed in the other thinning fluids; the only exception was the $n = 0.32$ fluid with the smallest capillary diameter for which the mean bubble diameter was 36% higher than all the other cases.

4.4. Mean bubble velocity and drag coefficient

Fig. 8 shows the ratio of the mean bubble velocity with the single bubble velocity as a function of the gas fraction; the three bubble sizes produced in the bubble column are included. The theoretical values reported by Gummalam and Chhabra [28,35] for creeping and high Re flows ($100 < Re < 300$) are also shown for their lowest flow index values and for their Newtonian results.

The experimental and theoretical results agree in that the $\bar{U}_{SW}/U_{SI}$ curve has a positive slope for small gas fraction, in contrast to the result in Newtonian fluids. This means that, unlike the Newtonian flows, the hydrodynamic hindrance produced by bubbles interactions does not produce a reduction of the bubble velocity with Φ_g; in the shear-thinning cases this effect is compensated by the reduction of the apparent viscosity produced by the local shear rate values. Hence, the Happel cell model used by Gummalam and Chhabra [28,35] captures the basic nature of these flow types. This fact also agrees with the early results of Buchholz et al. [18].

The values of the gas volume fraction for which the maximum of the $\bar{U}_{SW}/U_{SI}$ value was observed in the experiments were, nevertheless, much smaller than the theoretical ones. In fact for $\Phi_g > 1\%$ the heterogeneous regime is observed, that is why measurements at higher volumetric flow rates or gas fractions (where the maximum theoretical values were found) are practically impossible to attain in a bubbly flow regime.

Additionally, the experimental values of the velocities ratios were found to be much larger than the theoretical ones. As the bubble size decreases, the difference between the theoretical and experimental values increases (up to nine times for the case of the $n = 0.57$ fluid, see Fig. 8c). Hence, the Happel cell model is not sufficient to explain the whole phenomenon. The effect which is not accounted for in this model is the appearance of bubble clusters (like those shown in Fig. 6c and d). These clusters are responsible for the high $\bar{U}_{SW}/U_{SI}$ values found in the experiments. The shape of the curves in Fig. 8 indicates that the clusters grow up to a certain size just before the transition to the heterogeneous regime.

The last important difference is that while in the theoretical results the velocity ratio increases monotonically with the thinning behavior (decreasing the flow index value), the experimental results do not necessarily follow this trend. For instance, in Fig. 8a and b the curves of the fluids with $n = 0.85$ and 0.32 are closed to the theoretical ones while the fluids with $n = 0.55$ and 0.76 are far from them due to the formation of clusters.

The values of the drag coefficient (in terms of a drag correction factor $X = C_d Re/24$) were also reported in the theoretical work of Gummalam and Chhabra [28]. Their results showed that the C_d increases with the gas volume fraction for $n > 0.4$, as is commonly observed, but decrease for index flow values below 0.4. In [35] the C_d values for $Re = 50$ were also reported. These authors mentioned that the C_d increases with the gas volume fraction, obtaining again the common trend found in [28]. In a recent numerical work of the same group [10], where the Happel cell model was also used, the C_d values were found to increase with the gas fraction at the same n value although such increase was found to be negligible for $\Phi_g < 0.001$. In the present work an estimation of the C_d values of the bubbly flows were also obtained for low gas volume fractions. We computed the C_d values using Eq. (5) with the values of the mean bubble diameter and velocity of the flow. For comparison, we also calculated the C_d using the constitutive equation proposed by Ishii

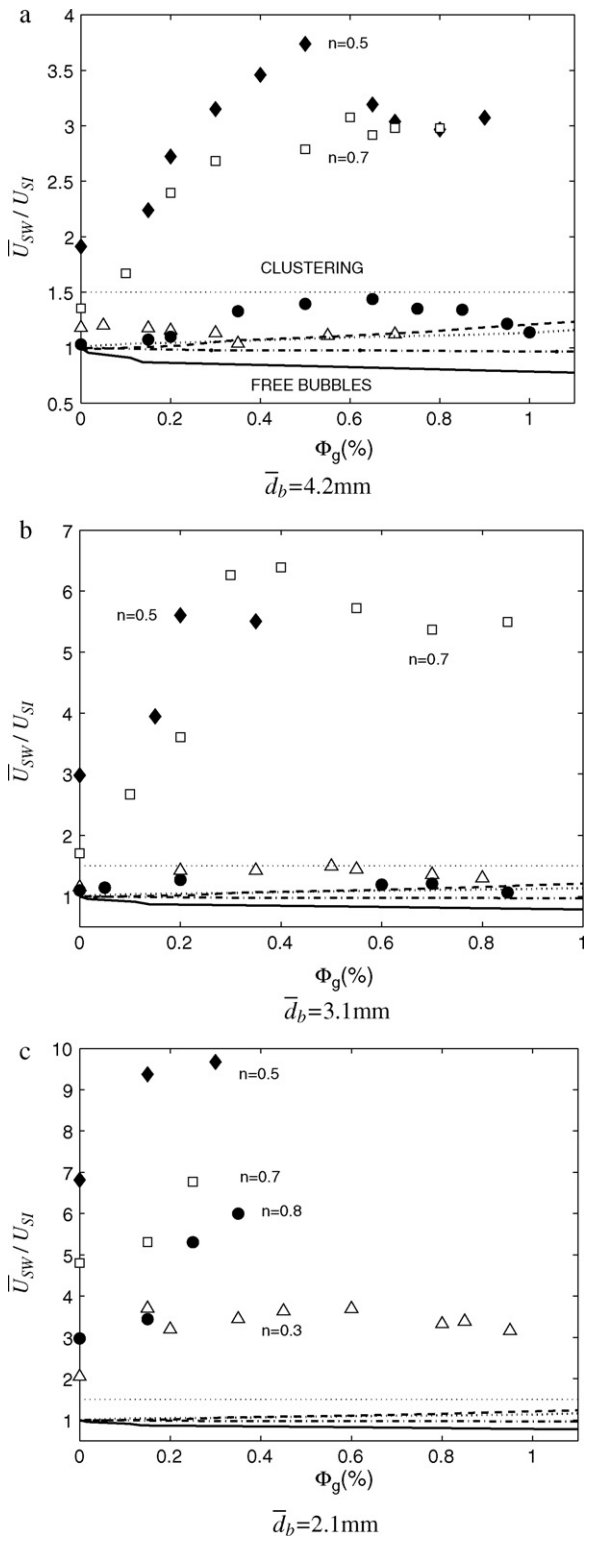

Fig. 8. $\bar{U}_{SW}/U_{SI}$ ratio as a function of the gas hold up Φ_g for the three mean bubble diameters. (•) $n = 0.85$, (□) $n = 0.76$, (♦) $n = 0.55$, (△) $n = 0.32$, theoretical values [28,35]: (–) creeping flow $n = 1.0$, (···) creeping flow $n = 0.3$, (-·-) $100 < Re < 300$ $n = 1.0$, (– –) $100 < Re < 300$ $n = 0.2$. The dotted horizontal line at 1.5 divides the free bubble and cluster formation regimes.

Table 3
Drag coefficient values for different thinning fluids and gas volume fractions. In order to calculate $C_d(Re_{SI})$ of Eq. (6) the respective bubble diameter obtained in the bubble column was used. The data of Kishore et al. [10] corresponds to the C_d values found for $n = 0.6$ and 0.8 and a gas fraction of 0.001.

n	Φ_g	Re	C_d	C_d Eq. (6)	C_d Ref. [10]
0.32	0.001	10.3	3.9	4.2	
	0.002	10.9	3.6	3.9	
	0.003	10.9	2.8	3.6	
0.55	0.001	5.2	2.6	6.0	4.0
	0.003	5.8	2.3	5.3	
0.76	0.001	3.6	4.2	8.0	5.5
	0.002	4.2	3.3	6.5	
	0.007	4.3	2.8	6.0	

and Zuber [41]:

$$C_d = C_d(Re_{SI})\left(\frac{U_{SI}}{U_{SW}}\right)^2\left(1-\Phi_g\right) \tag{6}$$

where the functional dependance of $C_d(Re_{SI})$ was obtained using the single bubble data for each fluid (Fig. 4). This equation was proposed considering a multiparticle system moving in one dimension in an infinite medium (absence of walls). The results are shown in Table 3.

It can be observed that the drag coefficient actually decreases as the gas volume fraction increases for the same fluid and *Re* number, unlike the general trend found by Kishore et al. [10]. Such decrease of the C_d is directly related to cluster formation and growth. Unlike the Newtonian fluids, where the C_d increases with the gas fraction, in bubbly shear-thinning fluids it decreases. It can be seen that Eq. (6) and the numerical results of Kishore et al. [10] both overestimate the values of C_d because they do not consider interactions or associations between bubbles.

4.5. Cluster size

The equivalent cluster diameter $\bar{d}_c$ for one of the thinning fluids ($n = 0.76$) is presented in Fig. 9 as a function of the gas volume fraction. In this plot the $\bar{d}_c$ values produced by the smallest and largest capillaries are shown both in dimensional and dimensionless form (scaled by the bubble diameter $\bar{d}_b$). The ratio $(\bar{d}_c/\bar{d}_b)^3$ was used because it is directly proportional to the number of bubbles in a cluster. In this particular fluid clusters were observed for the three bubble sizes tested, that is, bubble clusters are formed no matter what the value of the $\bar{d}_b$ is. Also in this fluid we had the opportunity to take more data of the cluster diameters before the heterogeneous regime occurred. For the $n = 0.55$ fluid the transition to this regime occurs at lower gas volume fractions. On the one hand we can observe in Fig. 9a that the cluster size and growth rate is the same for the two bubble diameters, suggesting that the size of the clusters is mainly determined by the fluid properties, channel width and the amount of available gas. On the other hand, we verified (Fig. 9b) that the number of bubbles embedded in the cluster is larger for the case of the small bubbles than the larger ones. Additionally, we found that the normalized standard deviation of the cluster size ($\sigma/\bar{d}_b$) is larger for the small bubble (up to ± 123) in comparison to the large bubble case (up to ± 5), indicating that the clusters made with the small bubbles interchange bubbles more often with their surroundings.

4.6. Bubble velocity variance

We can expect that bubble cluster formation will affect the agitation levels in the liquid; hence, a larger bubble velocity variance will be present in comparison with flows where no clusters are found. To verify this argument the bubble velocity variance was measured. The normalized values of the variance ($T_b/\bar{U}_{SW}^2$) for the

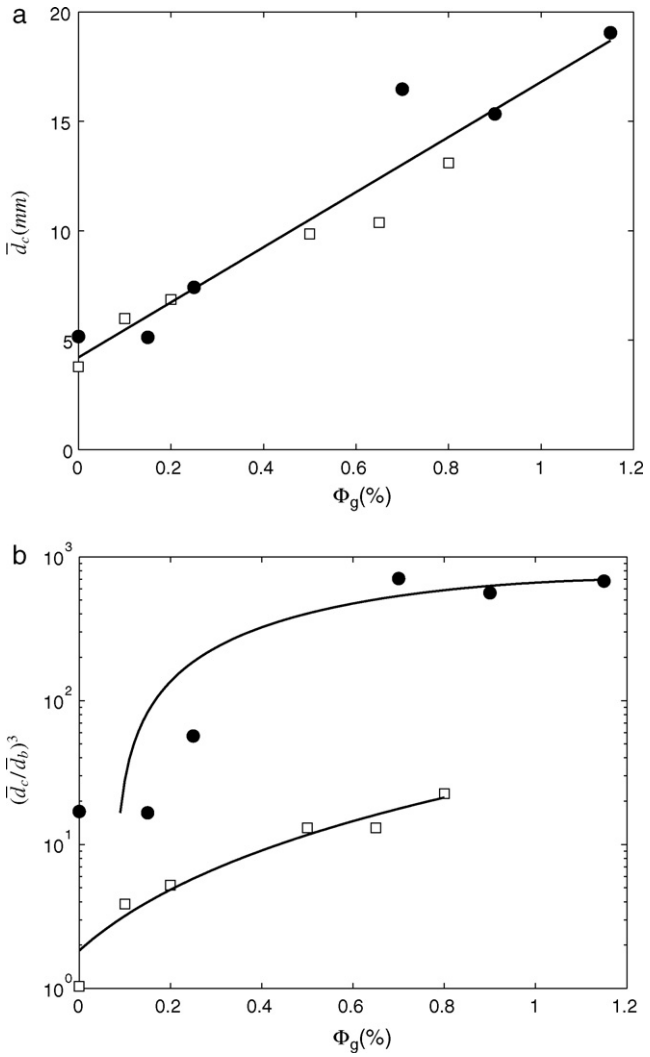

Fig. 9. Mean equivalent cluster diameter $\bar{d}_c$ as a function of Φ_g for the $n = 0.76$ fluid. In (b) the values are divided by the mean equivalent bubble diameter $\bar{d}_b$ and elevated to the third power. (•) $\bar{d}_b = 2.1$ mm, (□) $\bar{d}_b = 4.2$ mm. The lines are only visual aids.

thinning fluid with $n = 0.85$ were determined for the three bubble diameters; these results are shown in Fig. 10. For this fluid no cluster formation was observed for the medium and large bubbles; clusters appeared only with the smaller bubble size (see Fig. 8). As can be observed in Fig. 10, the normalized bubble velocity variances for the medium and large bubbles ($4 < Re < 14$) are in agreement with the values obtained by Martínez-Mercado et al. [8] for a Newtonian fluid with similar *Re* values ($10 < Re < 30$). In the case of the smaller bubbles (2.1 mm, with $1.7 < Re < 3.4$), where clusters are formed, the $T_b/\bar{U}_{SW}^2$ values surpass by nearly one order of magnitude the values achieved by the unclustered cases. This cluster-fluctuation relation seen at low *Re* numbers is very different from that expected in potential flows [36]. A common feature in high *Re* flows is that clustering is suppressed by bubble velocity fluctuations [16]. In the present study, fluctuations are enhanced by the clusters. Such difference adds to the already large list of the contrasting behavior between inertial and viscous dominated flows. Similar $T_b/\bar{U}_{SW}^2$ values and behavior were obtained for the other thinning fluids.

It is interesting to note that the values of the bubble velocity variance found here for a range of $1.7 < Re < 3.4$ and thinning conditions are of the same magnitude as the liquid velocity variance found by Cartellier and Rivière [42] for similar *Re* values ($0.66 < Re < 1.48$) and gas fractions in Newtonian fluids, although in their experiments the

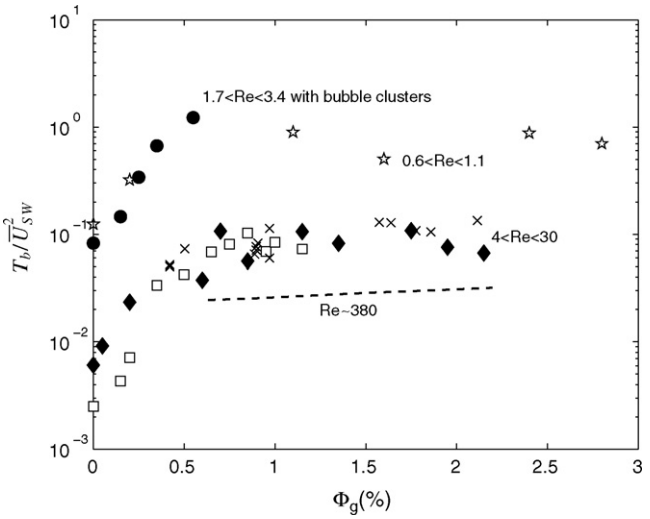

Fig. 10. Bubble velocity variance T_b divided by $\bar{U}_{SW}^2$ as a function of Φ_g. Experimental values of this work: (•) $\bar{d}_b = 2.1$ mm, $n = 0.85$; (♦) $\bar{d}_b = 3.1$ mm, $n = 0.85$; (□) $\bar{d}_b = 4.2$ mm, $n = 0.85$; (⋆) $\bar{d}_b = 2.1$ mm, Newtonian fluid. Other experimental values: (×) data taken from [8] with Newtonian fluids, (– –) data taken from [17].

liquid phase was forced to flow in a co-current manner with the gas phase. Cartellier et al. [43] observed that the dispersion was composed by free bubbles, bubble pairs, some triplets and clusters composed by more than five bubbles, and also reported a gas concentration increase at the center of the column. As the volumetric gas flow rate was further increased, the gas fraction profile gained the classical saddle shape, that is, with wall peaked distributions, and bubble aggregates were dissociated. Although in the present work the types of bubble associations mentioned by Cartellier et al. [43] in a Newtonian fluid was not observed, the $\bar{U}_{SW}/U_{SI}$ ratios obtained with this fluid with the smallest and medium bubble diameters were higher than one (up to 1.3) in the limit of zero gas fraction, contrary to that observed by Zenit et al.[17], reveling a kind of long distance interaction between bubbles. In addition to this, the bubble velocity variance measured for the Newtonian fluid at low *Re* numbers ($0.6 < Re < 1.1$) also surpassed by nearly one order of magnitude the values of more inertia dominated flows [8] (see Fig. 10).

From all this evidence we can argue that in viscous dominated bubbly flows (in both Newtonian and thinning fluids) the long range interactions promote the increase of the rise velocity of the bubbles comparing with the single bubble value. This kind of behavior is similar to the one seen with settling particles [20,21]. Other effects of these viscous flows could be the increase of bubble fluctuations, precisely due to the long range bubble interactions, and a net repulsion force between the bubbles and the column walls [44], which could explain the abnormal gas fraction profiles obtained by Cartellier et al. [43]. Clustering in thinning fluids has, however, important differences with the one observed in Newtonian fluids: the number of bubbles embedded in the cluster is higher in comparison with the number of bubbles found in the Newtonian case; the compactness of the clusters is also higher in the case of the thinning fluids. We think that cluster growth in thinning fluids is a mechanism that reduces the spatial viscosity differences in the flow leading to a 'Newtonian-like' state as the gas fraction is increased. This idea is explained in the companion paper [23].

5. Conditions for cluster formation

As we saw in Section 4.4, the increase of the velocity ratio $\bar{U}_{SW}/U_{SI}$, due to bubble clustering, does not depend directly on the value of the flow index *n*. This means that a more thinning fluid does not necessarily induces bubble clustering. We found that a combination of the values of the Reynolds and Eötvös numbers give the conditions for cluster formation. The value of the flow index is taken into account in the apparent viscosity included in the *Re* number. This kind of dependence of the forces acting on the bubbles with the flow index is in agreement with the results of Zhu et al. [34], who work with thinning fluids that were forced to pass through a fixed arrangement of rigid spheres. They found that the drag force experimented on a test particle does not depend on the values of the flow index but in the Reynolds number and the spacing between particles.

To identify the hydrodynamic conditions for which bubble clusters are formed we show our results in terms of the Reynolds and Eötvös numbers for the single bubble cases (using Fig. 4), the *Eo* (also known as Bond) number being defined as:

$$Eo = \frac{\rho g d_b^2}{\sigma} \tag{7}$$

For the case of isolated bubbles the *Eo*–*Re* plot is often used to identify the shapes of the bubbles [45]. Cluster formation can be identified by direct observation of the bubbly flow and also by evaluating the change of $\bar{U}_{SW}/U_{SI}$ with the gas volume fraction. When the velocity ratio is larger than 1.5, cluster formation was observed. In Fig. 8a, for example, bubble clusters are formed in the $n = 0.5$ and 0.7 fluids; in Fig. 8c all the thinning fluids formed bubble clusters since $\bar{d}_b$ was small. The relation $\bar{U}_{SW}/U_{SI} = 1.5$ only serves as a distinction between the condition where the velocity of the bubble swarms was higher than the single velocity but without the formation of clusters, as in the Newtonian fluid. We identified cluster formation mainly by simple observation. In the case of the $n = 0.32$ fluid with the smaller bubbles (2.9 mm), cluster identification was not easy at gas fractions around 0.4%. At this value clusters become progressively diluted by the whole flow. Nevertheless, we recognized these flows as part of the clustering condition since the values of $\bar{U}_{SW}/U_{SI}$ were above 1.5.

Another parameter that can be used to recognize bubble clustering is the bubble velocity variance. As shown in Section 4.6, bubble clustering increases considerably the velocity variance of the liquid and bubbles. In our bubbly flows the normalized standard deviation $\sqrt{T_b/\bar{U}_{SW}^2}$ was about ±0.4 in unclustered flows while it reached up to ±5.0 when clusters were formed.

The result of this mapping is shown in Fig. 11; it includes the five fluids used in this work. We can describe this plot as follows: the data is separated according to the clustering behavior, filled and empty symbols show flow conditions where clustering was or was not detected, respectively. For instance, a filled symbol was assigned to a *Eo*–*Re* point if for the same bubble diameter and liquid properties the bubbles clustered for a particular gas volume fraction. This mapping is easy to do because the gradual increase of the gas fraction produce only a slight increase of $\bar{d}_b$. A separation of the two regimes can be observed. Clearly, the clustering is observed when the viscous effects are more important than the inertial ones (small Re). Hence, as inertia increases it is possible to break the clustering behavior. Additionally, the deformability of the bubbles is also important. For a given value of Re, a flow with more deformable bubbles will tend to cluster more easily (as the *Eo* increases). The separation between the two regimes is given approximately by the iso-Morton line of 1×10^{-3}, the Morton number being defined as:

$$Mo = \frac{g\eta^4}{\rho\sigma^3} \tag{8}$$

Previously, a Morton value of 4×10^{-4} was proposed [9,46] as a transition indicator from non-coalescing flows to coalescing flows in Newtonian fluids. This suggest that the transition of non-interacting to interacting bubbles is a general condition for inelastic fluids, including the Newtonian and shear-thinning fluids. In this

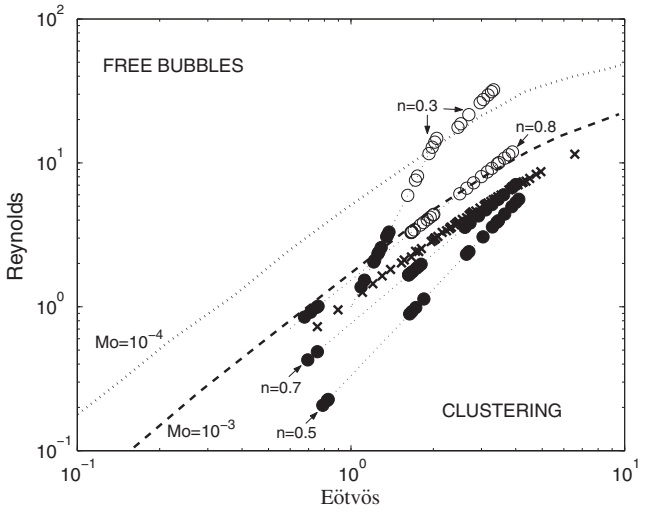

Fig. 11. Cluster condition formation mapped in a *Eo*–*Re* curve of the single bubbles. (•) hydrodynamic conditions for bubble clustering, (○) hydrodynamic conditions for free bubbles, (– –) $Mo = 10^{-3}$, (. . .) $Mo = 10^{-4}$, (×) Newtonian values. The iso-Morton lines were taken from [45].

work no clustering was seen at first glance in the Newtonian fluid. Nevertheless, a pair of bubbles rising in a viscous Newtonian fluid can form a stable doublet (see the companion paper [23]). This indicates that the gas fraction has an important role in cluster desegregation in Newtonian fluids, as seen by Cartellier et al. [43].

The *Mo* number increases from top to bottom in a *Eo*–*Re* plot. The tendency to form bubble clusters increases with the Morton number. That is why the $n = 0.55$ fluid, with the highest *Mo* number, has the biggest $\bar{U}_{SW}/U_{SI}$ values (see Fig. 8) followed by the $n = 0.76$ fluid and finally by the $n = 0.85$ and 0.32 fluids.

We could infer from Fig. 11 that at very low *Re* numbers, in the creeping flow regime, the curves displayed in Fig. 8 will have the same trend as the theoretical ones, that is to say, the $n = 0.32$ fluid will have the highest $\bar{U}_{SW}/U_{SI}$ values, as it will have the highest Morton number, followed by the $n = 0.55$ and so on. As discussed by other authors [47,46], bubble interaction strongly depends on the bubbles wake and vortices structure, which in turn evolve as the *Re* number is increased or the bubble shape is changed. Additionally, the degree of deformation of a bubble, measured with the Eötvös (or Bond) number is another important factor that enhance bubble alignment and coalescence, as explained by Manga and Stone [48,49]. In this work a maximum *Eo* number of 10 was reached. It would be interesting to investigate if bubbles with $Eo > 40$ and $Mo > 1 \times 10^{-3}$, in which according to [45] the skirted and dimpled ellipsoidal-cap bubbles are observed, also form clusters in thinning fluids.

In the companion paper of this investigation [23] we present a detailed study of the interaction of two bubbles rising in the same shear-thinning fluids employed in this work. The results, which pointed out the importance of the shear-thinning wake formed by a leading bubble, complement and explain the appearance of bubble clusters in thinning fluids whose structure differs significantly from the ones observed in Newtonian bubbly flows.

6. Conclusions

In this work experiments were conducted to study cluster formation in bubbly flows with shear-thinning fluids. Special care was taken to produce nearly mono-dispersed bubbly flows and to employ thinning fluids with negligible elasticity. The visual observation of the flow revealed the formation of dense bubble clusters in the thinning fluids which grow with the gas fraction and increase the mean bubble velocity with respect to the velocity achieved by single bubbles. Such clusters, which actually lead to contact between bubbles, have larger dimensions and lifetime than the ones observed in Newtonian potential flows [16,17]. By measuring the mean rise velocity of the bubble swarms $\bar{U}_{SW}$ at different gas fractions, and non-dimensionalized them with the single bubble velocities U_{SI}, comparison with previous theoretical data could be conducted. The main conclusions of this investigation are:

1. Qualitative agreement of the velocities ratio $\bar{U}_{SW}/U_{SI}$ as a function of the gas volume fraction was found with the theoretical studies [28,35]. Therefore, the Happel cell model can predict the effects of the reduction of the local viscosity together with the hydrodynamic hindrance provoked by bubble interactions.
2. Quantitative agreement with the velocities ratio was not found between the experiments of this work and the theoretical predictions since the maximum of the velocity ratio $\bar{U}_{SW}/U_{SI}$ was found at lower gas fractions than the ones predicted by the theory, which this work revealed that is was incomplete. In fact, the permissible experimental gas fraction values are much lower than the theoretical ones for the cases of mono-dispersed bubbly flows. The heterogeneous or churn-turbulent regime has interesting issues by itself but cannot be used to compare experimental results with the available theoretical data.
3. The magnitude of the velocity ratio $\bar{U}_{SW}/U_{SI}$ was higher than the theoretical one even at low values of the gas fraction. The difference is attributed to the formation of clusters which the Happel cell model does not account for.
4. The ratio of the mean bubble velocity and the single bubble velocity did not follow an orderly correspondence with the flow index values, as seen in the theoretical works. Instead of this, the $\bar{U}_{SW}/U_{SI}$ values could be related to the values of the Reynolds and Eötvös numbers of the single bubbles. Moreover, the bubble clustering condition was mapped in a *Eo*–*Re* plot. Two regimes were identified: a free bubble regime and a cluster formation regime. The limit between one and the other is close to a critical Morton number (4×10^{-4}) which has been identified as a transition indicator from non-coalescing flows to coalescing flows in Newtonian fluids.

We should mention that although the *Eo*–*Re* plot proved to be useful in predicting bubble clustering using single bubble data, it could underestimate the roll that the gas fraction has on cluster growth. The influence of the gas fraction, which seems to be important in Newtonian fluids and lesser in shear-thinning fluids, should be clarified in the future.

Measurements were also conducted to obtain the equivalent diameter of the bubble cluster and bubble velocity variance. These results suggest that the cluster growth is not related to the size of individual bubbles and that the dimensionless bubble velocity variance $T_b/\bar{U}_{SW}^2$ increases significantly when bubble clusters are formed.

It is our hope that this work will contribute to the understanding of the formation of bubble clusters in shear-thinning fluids, which is an important issue in multiphase flows as well as a precursor to bubble coalescence and change of regime in bubble flows.

Acknowledgements

The authors will like to thank the support of G. Sánchez, F. Calderas and L. Medina for their help in the rheological measurements. R. Vélez acknowledges CONACyT-México for its financial support during his doctoral studies.

References

[1] N. Kantarci, F. Borak, K.O. Ulgen, Bubble column reactors, Proc. Biochem. 40 (2005) 2263.
[2] W.-D. Deckwer, Bubble Column Reactors, Wiley, NY, 1992.
[3] Y.T. Shah, B.G. Kelkar, S.P. Godbole, W.-D. Deckwer, Design parameters estimation for bubble column reactors, A. I. Ch. E. J. 28 (1982) 353.
[4] M. Zlokarnik, Trends and needs in bioprocess engineering, Chem. Eng. Prog. 86 (1990) 62.
[5] H.W. Blanch, S.M. Bhavaraju, Rheology of fermentation broths, Biotechnol. Bioeng. 18 (1976) 745.
[6] P.M. Kilonzo, A. Margaritis, The effects of non-Newtonian fermentation broth viscosity and small bubble segregation on oxygen mass transfer in gas-lift bioreactors: a critical review, Biochem. Eng. J. 17 (2004) 27.
[7] L. van Wijngaarden, On pseudo turbulence, Theor. Comput. Fluid Dynam. 10 (1998) 449.
[8] J. Martínez-Mercado, C.A. Palacios-Morales, R. Zenit, Measurement of pseudo-turbulence intensity in monodispersed bubbly liquids for $10 < Re < 500$, Phys. Fluids 19 (2007) 103302.
[9] A. Smolianski, H. Haario, P. Luukka, Numerical study of dynamics of a single bubbles and bubbles swarm, Appl. Math. Model. 23 (2008) 641.
[10] N. Kishore, R.P. Chhabra, V. Eswaran, Drag on ensembles of fluid spheres translating in a power-law liquid at moderate Reynolds numbers, Chem. Eng. J. 139 (2008) 224.
[11] S. Radl, G. Tryggvason, J.G. Khinast, Flow and mass transfer of fully resolved bubble in non-Newtonian fluids, A. I. Ch. E. J. 53 (2007) 1861.
[12] R.G. Larson, The Structure and Rheology of Complex Fluids, Oxford University Press, 1999.
[13] H.H. Hu, N.A. Patankar, M.Y. Zhu, Direct numerical simulations of fluid–solid systems using the arbitrary Lagrangian–Eulerian technique, J. Comput. Phys. 169 (2001) 427.
[14] G. Gheissary, B.H.A.A. van den Brule, Unexpected phenomena observed in particle settling in non-Newtonian media, J. Non-Newton. Fluid Mech. 67 (1996) 1.
[15] D.D. Joseph, Y.J. Liu, M. Poletto, J. Feng, Aggregation and dispersion of spheres falling in viscoelastic liquids, J. Non-Newton. Fluid Mech. 54 (1994) 45.
[16] B. Figueroa-Espinoza, R. Zenit, Clustering in high *Re* monodispersed bubbly flows, Phys. Fluids 17 (2005) 091701.
[17] R. Zenit, D.L. Koch, A.S. Sangani, Measurements of the average properties of a suspension of bubbles rising in a vertical channel, J. Fluid Mech. 429 (2001) 307.
[18] H. Buchholz, R. Buchholz, J. Lücke, K. Schügerl, Bubble swarm behavior and gas absortion in non-Newtonian fluids in sparged columns, Chem. Eng. Sci. 33 (1978) 1061.
[19] A. Schumpe, W.-D. Deckwer, Gas holdups, specific interfacial areas, and mass transfer coefficients of aerated carboxymethyl cellulose solutions in a bubble column, Ind. Eng. Chem. Proc. Des. Dev. 21 (1982) 706.
[20] K.O.L.F. Jayaweera, B.J. Mason, G.W. Slack, The behavior of cluster of spheres falling in a viscous fluid, J. Fluid Mech. 20 (1964) 121.
[21] L.M. Hocking, The behavior of clusters of spheres falling in a viscous fluid, J. Fluid Mech. 20 (1964) 129.
[22] D.D. Joseph, Y.J. Liu, Orientation of long bodies falling in a viscoelastic liquid, J. Rheol. 37 (1993) 961.
[23] J.R. Vélez-Cordero, D. Samano, P. Yue, J.J. Feng, R. Zenit, Hydrodynamic interaction between a pair of bubbles ascending in shear-thinning inelastic fluids, J. Non-Newton. Fluid Mech., submitted for publication.
[24] W.-D. Deckwer, K. Nguyen-tien, A. Schumpe, Y. Serpemen, Oxygen mass transfer into aerated CMC solutions in a bubble column, Biotechol. Bioeng. 24 (1982) 461.
[25] S.P. Godbole, A. Schumpe, Y.T. Shah, N.L. Carr, Hydrodynamics and mass transfer in non-Newtonian solutions in a bubble column, A. I. Ch. E. J. 30 (1984) 213.
[26] N.W. Haque, K.D.P. Nigam, K. Viswanathan, J.B. Joshi, Studies on gas holdup and bubble parameters in bubble columns with (carboxymethyl)cellulose solutions, Ind. Eng. Chem. Res. 26 (1987) 86.
[27] N.W. Haque, K.D.P. Nigam, K. Viswanathan, J.B. Joshi, Studies on bubble rise velocity in bubble columns employing non-Newtonian solutions, Chem. Eng. Commun. 73 (1988) 31.
[28] S. Gummalam, R.P. Chhabra, Rising velocity of a swarm of spherical bubbles in a power law non-Newtonian liquid, Can. J. Chem. Eng. 65 (1987) 1004.
[29] S.M. Bhavaraju, R.A. Mashelkar, H.W. Blanch, Bubble motion and mass transfer in non-newtonian fluids: Part II. Swarm of bubbles in a power law fluid, A. I. Ch. E. J. 24 (1978) 1070.
[30] T. Hirose, M. Moo-Young, Bubble Drag and Mass Transfer in non-Newtonian Fluids: Creeping Flow with Power-law Fluids, Can. J. Chem. Eng. 47 (1969) 265.
[31] J. Happel, Viscous flow in multiparticle systems: slow motion of fluids relative to beds of spherical particles, A. I. Ch. E. J. 4 (1958) 197.
[32] D. Rodrigue, D. De Kee, C.F. Chan Man Fong, A note on the drag coefficient of a single gas bubble in a power-law fluid, Can. J. Chem. Eng. 77 (1999) 766.
[33] A. Acharya, R.A. Mashelkar, J. Ulbrecht, Mechanics of bubble motion and deformation in non-newtonian media, Chem. Eng. Sci. 32 (1977) 863.
[34] C. Zhu, K. Lam, H.-H. Chu, X.-D. Tang, G. Liu, Drag forces of interacting spheres in power-law fluids, Mech. Res. Commun. 30 (2003) 651.
[35] R.P. Chhabra, Rising velocity of a swarm of spherical bubbles in power law fluids at high Reynolds numbers, Can. J. Chem. Eng. 76 (1998) 137.
[36] P.D.M. Spelt, A.S. Sangani, Properties and averaged equations for flows of bubbly liquids, Appl. Sci. Res. 58 (1998) 337.
[37] H.N. Oğuz, A. Prosperetti, Dynamics of bubble growth and detachment from a needle, J. Fluid Mech. 257 (1993) 111.
[38] R.R. Lessard, S.A. Zieminski, Bubble coalescence and gas transfer in aqueous electrolytic solutions, Ind. Eng. Chem. Fundam. 10 (1971) 260.
[39] F. Calderas, A. Sanchez-Solis, A. Maciel, O. Manero, The transient flow of the PET-PEN-montmorillonite clay nanocomposite, Macromol. Symp. 283–284 (2009) 354.
[40] E. Soto, C. Goujon, R. Zenit, O. Manero, A study of velocity discontinuity for single air bubbles rising in an associative polymer, Phys. Fluids 18 (2006) 121510.
[41] M. Ishii, N. Zuber, Drag coefficient and relative velocity in bubbly, droplet or particulate flows, A. I. Ch. E. J. 25 (1979) 843.
[42] A. Cartellier, N. Rivière, Bubble-induced agitation and microstructure in uniform bubbly flows at small to moderate particle Reynolds numbers, Phys. Fluids 13 (2001) 2165.
[43] A. Cartellier, L. Timkin, N. Rivière, New structures of Poiseuille bubbly flows due to clustering, in: Proc. ASME-FEDSM' 97, paper 3528, Vancouver, June 22–26, 1997.
[44] P. Vasseur, R.G. Cox, The lateral migration of spherical particles sedimenting in a stagnant bounded fluid, J. Fluid Mech. 80 (1977) 561.
[45] R. Clift, J.R. Grace, M.E. Weber, Bubbles, Drops, and Particles, Academic Press, NY, 1978.
[46] C.W. Stewart, Bubble interaction in low-viscosity liquids, Int. J. Multiphase Flow 21 (1995) 1037.
[47] D. Legendre, J. Magnaudet, G. Mougin, Hydrodynamic interactions between two spherical bubbles rising side by side in a viscous liquid, J. Fluid Mech. 497 (2003) 133.
[48] M. Manga, H.A. Stone, Buoyancy-driven interactions between two deformable viscous drops, J. Fluid Mech. 256 (1993) 647.
[49] M. Manga, H.A. Stone, Collective hydrodynamics of deformable drops and bubbles in dilute low Reynolds number suspensions, J. Fluid Mech. 300 (1995) 231.